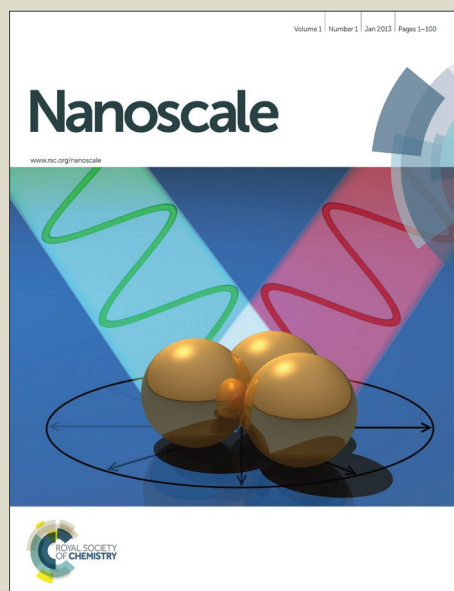


# Nanoscale

Accepted Manuscript



This is an *Accepted Manuscript*, which has been through the Royal Society of Chemistry peer review process and has been accepted for publication.

*Accepted Manuscripts* are published online shortly after acceptance, before technical editing, formatting and proof reading. Using this free service, authors can make their results available to the community, in citable form, before we publish the edited article. We will replace this *Accepted Manuscript* with the edited and formatted *Advance Article* as soon as it is available.

You can find more information about *Accepted Manuscripts* in the [Information for Authors](#).

Please note that technical editing may introduce minor changes to the text and/or graphics, which may alter content. The journal's standard [Terms & Conditions](#) and the [Ethical guidelines](#) still apply. In no event shall the Royal Society of Chemistry be held responsible for any errors or omissions in this *Accepted Manuscript* or any consequences arising from the use of any information it contains.



Journal Name

ARTICLE

## Ab initio study of nickel-catalyzed transformation of amorphous carbon into graphene in rapid thermal processing

Shuang Chen,<sup>ab</sup> Wei Xiong,<sup>c</sup> Yunshen Zhou,<sup>c</sup> Yongfeng Lu<sup>c</sup> and Xiao Cheng Zeng<sup>\*a</sup>

Received 00th January 20xx,  
Accepted 00th January 20xx

DOI: 10.1039/x0xx00000x

www.rsc.org/

*Ab initio* molecular dynamics (AIMD) simulations are employed to investigate chemical mechanism underlying the Ni-catalyzed transformation of amorphous carbon (*a*-C) into graphene in the rapid thermal processing (RTP) experiment to directly grow graphene on various dielectric surfaces *via* the evaporation of surplus Ni and C at 1100°C (below the melting point of bulk Ni). It is found that the *a*-C-to-graphene transformation entails the metal-induced crystallization and layer exchange mechanism, rather than the conventional dissolution/precipitation mechanism typically involved in Ni-catalyzed chemical vapor deposition (CVD) growth of graphene. The multi-layer graphene can be tuned by changing the relative thicknesses of deposited *a*-C and Ni thin films. Our AIMD simulations suggest that the easy evaporation of surplus Ni with excess C is likely attributed to the formation of *viscous-liquid-like* Ni-C solution within the temperature range of 900–1800 K and to the faster diffusion of C atoms than that of Ni atoms above 600 K. Even at room temperature, *sp*<sup>3</sup>-C atoms in *a*-C are quickly converted to *sp*<sup>2</sup>-C atoms in the course of simulation, and the graphitic C formation can occur at low temperature. When the temperature is as high as 1200 K, the grown graphitic structures reversely dissolve into Ni. Because the rate of temperature increase is considerably faster in the AIMD simulations than in realistic experiments, defects in the grown graphitic structures are kinetically trapped. In this kinetic growth stage, the carbon structures grown from *sp*<sup>3</sup>-carbon or from *sp*<sup>2</sup>-carbon exhibit marked differences.

### 1. Introduction

Graphene is a highly desired two-dimensional (2D) material due to its exceptional electronic, optical, and mechanical properties.<sup>1–3</sup> For industrial applications, however, large-area and high-quality graphene is demanded at low cost. To date, many experimental approaches have been developed to produce graphene, including mechanical exfoliation,<sup>4</sup> liquid-phase exfoliation,<sup>5</sup> chemical exfoliation *via* graphene oxide,<sup>6,7</sup> epitaxial growth on silicon carbide,<sup>8,9</sup> and metal-catalyzed chemical vapor deposition (CVD).<sup>10–12</sup> Among these approaches, the metal-catalyzed CVD has been widely used to fabricate large-area and high-quality graphene.<sup>13–15</sup> Correspondingly, previous theoretical investigations of graphene growth have been mainly focused on the CVD growth. It is known that the CVD growth of graphene is substrate-, carbon-feedstock-, and growth-condition-

dependent. To optimize the experimental CVD parameters, in-depth understanding of the CVD growth mechanism at the atomic level is desired. Two common metal catalysts for the CVD growth are Ni and Cu. Accordingly, two widely accepted but different CVD growth mechanisms are the carbon segregation/precipitation process in Ni with high carbon solubility, and the surface adsorption process on Cu with negligible bulk solubility.<sup>16</sup> Due to the huge time- and length-scale differences between realistic experiments and molecular simulation studies to describe the graphene growth mechanism, simulations typically focus on a specific aspect of the CVD growth.

Previous theoretical studies of CVD growth of graphene mostly employed three computational methods: *ab initio* computation, molecular dynamics (MD) and Monte Carlo (MC) simulations, and multi-scale hybridized methods. *Ab initio* computation can predict quantitative reaction barriers in certain chemical processes that are involved in the graphene growth, especially for dehydrogenation of gaseous carbon feedstock on metal surfaces.<sup>17–19</sup> It can also assess relative energies of well-designed models, targeted to some specific problems such as suppression of grain boundaries by Cu-Mn alloy<sup>20</sup> and graphene edge stabilization by Au atom on Ni(111) step.<sup>21</sup> Ding and coworkers used density functional theory (DFT) calculations to study thermodynamic and kinetic aspects associated with special processes in the graphene growth, such as preference of graphene nucleation near the Ni(111) step edge,<sup>22</sup> the C<sub>21</sub> precursor in CVD growth of graphene,<sup>23</sup>

<sup>a</sup>Department of Chemistry, University of Nebraska–Lincoln, Lincoln, Nebraska 68588, United States

<sup>b</sup>Kuang Yaming Honors School, Nanjing University, Nanjing, Jiangsu 210023, China

<sup>c</sup>Department of Electrical and Computer Engineering, University of Nebraska–Lincoln, Lincoln, Nebraska 68588, United States

\*E-mail: xzeng1@unl.edu

Electronic Supplementary Information (ESI) available: Formation energies of Ni-Ni, Ni-C, and C-C atoms as a function of intermolecular distance in ESI Fig. S1, the whole super cells with vacuum layer of Model I and VIII in ESI Fig. S2, and initial and final configurations (ESI Fig. S3), MSD-time cures (ESI Fig. S4), diffusion coefficients (Table S1), and Lindemann Index (ESI Fig. S5) of four new models (VIII–XI) can be found there. See DOI: 10.1039/x0xx00000x

metal-surface-passivation-induced graphene edge reconstruction,<sup>24</sup> dominant zigzag edge of growing graphene on Cu surface,<sup>25</sup> vacancy formation and healing,<sup>26</sup> and effect of H<sub>2</sub> pressure on the formation of single-layer or multi-layer graphene.<sup>27</sup> To reproduce dynamical growth processes in CVD growth of graphene, the classical MD simulations combined with the reactive force-field (ReaxFF)<sup>28–30</sup> and the kinetic MC simulations (parameters derived from *ab initio* calculations)<sup>31</sup> were also used by a few groups. The non-equilibrium MD simulations with the second generation of Brenner potential, REBO2, was utilized to investigate reconstruction of divacancy in graphene under electron irradiation.<sup>32</sup> Ding and coworkers also run long-time MD simulations based on their developed REBO2 potential to investigate graphene growth on Ni(111) surface.<sup>33</sup> Moreover, the hybrid reactive MD/MC simulations were used to study the graphene formation through a combined deposition–segregation mechanism at different substrate temperatures and in the far-from-equilibrium high precursor flux condition.<sup>34</sup> The more accurate quantum mechanical MD simulations in the framework of the self-consistent-charge density-functional tight-binding (SCC-DFTB) method has been employed by Morokuma's group to investigate the dynamics of CVD growth of graphene, such as the pentagon-first mechanism and promotion of hexagonal ring formation in the presence of a coronene-like C<sub>24</sub> template in the initial nucleation stage on the Ni surface,<sup>35</sup> formation of graphene precursors underneath the Ni(111) surface,<sup>36</sup> catalysis comparison of Fe(111), Ni(111), and Cu(111) surfaces,<sup>37</sup> graphene nucleation from different nickel carbides,<sup>38</sup> malleable Ni(111) step edge,<sup>39</sup> and defeat healing on surface-molten copper.<sup>40</sup>

Thus far, only a few *ab initio* MD (AIMD) studies have been reported for the mechanistic study of graphene growth, largely due to very high computational cost and relatively short time scale (on the order of  $\sim 10^2$  ps) in AIMD.<sup>40–42</sup> In an early AIMD simulation based on the spin-polarized Perdew-Burke-Ernzerhof (PBE) functional with van der Waals (vdW) correction (PBE-D2) and projector augmented-wave (PAW) potentials, Ongun Özçelik *et al.* studied epitaxial growth of graphene without a substrate or on a boron-nitride substrate by adding C monomers or dimers to the edge of graphene platelet.<sup>41</sup> Shibuta *et al.* performed 5-ps AIMD simulation to study the CH<sub>4</sub> decomposition on Ni(111) surface at the initial stage of CVD growth.<sup>42</sup> They found that newly formed C monomers can be buried under the subsurface region to exhibit dissolution of C in Ni.<sup>42</sup> In this paper, we perform comprehensive AIMD simulations using the PBE-D3 functional with the Gaussian plane-wave (GPW) method, implemented in CP2K software package, to investigate atomic-scale mechanism of metal-catalyzed transformation of amorphous carbon (*a*-C) to the graphene in rapid thermal processing (RTP). The PBE-D3 method is shown to be quite accurate to describe the metal-metal, metal-carbon, and carbon-carbon interactions in the metal-carbon solution, on the basis of the computed formation energies of Ni-Ni, Ni-C, and C-C as a function of interatomic distance (see Electronic Supplementary Information (ESI) Fig. S1).

Our computational study is motivated from recent experimental studies of the metal-catalyzed transformation of *a*-C to graphene.<sup>43–47</sup> In particular, based on the single-step RTP, Xiong *et al.* successfully fabricated wafer-scale and high-quality graphene on various dielectric surfaces by direct evaporation of surplus Ni (typically  $\sim 65$  nm thin film) and excess *a*-C (typically 5 nm thin film) at an elevated temperature (1100°C).<sup>47</sup> The RTP approach can eliminate the post-growth treatment, the removal of metal substrate and graphene transfer, and limit the wrinkle formation in graphene.<sup>47</sup> To our knowledge, this is the first atomic-level simulation study of the growth mechanism of metal-catalyzed transformation of *a*-C into graphene in RTP. We are aware of one previous QM/MD study, using the non-consistent charge DFTB method, of the catalyst-free transformation of *a*-C to graphene.<sup>48</sup> Here, the more accurate and computationally more demanding AIMD simulations are performed to study the mechanism underlying the RTP growth of graphene from *a*-C. We found that the Ni-catalyzed transformation of *a*-C follows the metal-induced crystallization and layer exchange mechanism proposed from previous experimental study,<sup>44</sup> rather than the known dissolution/precipitation mechanism. We also found that when the temperature is higher than 600 K, C atoms diffuse faster than Ni atoms in the Ni-C solution. The easy evaporation of surplus Ni and C may be attributed to the formation of viscous-liquid-like Ni-C solution at 1100°C.

## 2. Computational details

### 2.1 *a*-C/Ni<sub>3</sub>C slab model setup

The Ni-catalyzed transformation of *a*-C to graphene by thermal annealing and cooling has been thoroughly investigated via experiments.<sup>43–46</sup> Note, however, that these experiments<sup>43–46</sup> differ from the RTP growth of graphene<sup>47</sup> in which the Ni thin film is directly evaporated at an elevated temperature (although the temperature is still below the melting point of bulk Ni) to fabricate the graphene on different dielectric surfaces. Regardless of whether the *a*-C layer is deposited prior to the deposition of Ni layer<sup>43</sup> or after,<sup>45</sup> the newly formed graphene is always on the top of the Ni layer. In a previous experimental study, Saenger *et al.* indicated that the *a*-C layer could be dissolved into the Ni layer during heating and expelled from solution upon cooling below the solid solubility limit, if the graphene growth from *a*-C followed the CVD dissolution/precipitation mechanism.<sup>44</sup> In fact, the graphitic C formation starts at temperatures of 640–730°C at which the C solubility in Ni is very low, suggesting that the graphitization is through a metal-induced crystallization and layer exchange mechanism, rather than the dissolution/precipitation mechanism.<sup>44</sup> For metal-induced crystallization, Saenger *et al.* proposed that C in Ni has a low concentration and high transport rate even at low temperature, and that the formation of crystalline C (more stable than *a*-C) on top of Ni layer can further induce continued dissolution of bottom *a*-C layer.<sup>44</sup> The *in situ* electron microscope study gives the same conclusion that the saturation of the metal with C and self-diffusion of C in the

metal precedes the nucleation and growth of graphene, and the transformation of  $a$ -C to the thermodynamically more favorable graphene occurs above 600°C, still at the heating stage.<sup>46</sup>

The growth of graphene in RTP<sup>47</sup> appears to follow a similar mechanism. Moreover, a new and important experimental evidence is the emergence of an intermediate  $\text{Ni}_3\text{C}$  phase in the temperature range of 200–800°C, which offers a new insight into the RTP-growth of graphene.<sup>49</sup> To understand the role of  $\text{Ni}_3\text{C}$  formation and the associated mechanism of graphene growth, we setup six slab models (Model I–VI) in Fig. 1a–f, viewed along the surface  $y$  axis. For each model, the slab dimensions are set to be  $12.8 \text{ \AA} \times 14.8 \text{ \AA} \times 40 \text{ \AA}$ , where the  $x$ - $y$  dimensions are the same as that of a graphene supercell containing 72 carbon atoms, and the vacuum layer along the  $z$  direction was cut to highlight reactive solid layers (the whole model system with vacuum layer ( $> 20 \text{ \AA}$ ) of Model I is depicted in ESI Fig. S2a).

In Model I or II (Fig. 1a and b), 72  $a$ -C atoms with 3/8 of them being  $sp^3$ -C atoms, or all of them being  $sp^2$ -C atoms are directly deposited on a  $\text{Ni}_3\text{C}$  layer with 96 atoms. The optimal thicknesses of  $a$ -C and Ni layers of 5 and 65 nm, respectively, are suggested from the RTP experiment to achieve high-quality graphene monolayer.<sup>47</sup> Both thicknesses are not feasible in our AIMD simulations. However, 72 C atoms and  $\text{Ni}_3\text{C}$  layer with 96 atoms in Model I and II yield a thickness of the solid layer to be about 17 Å while the ratio of thicknesses of  $\text{Ni}_3\text{C}$  layer to C layer is about 3.5. Both models are built to provide some insights into growth mechanism at nanoscale, mimicking the model system of a four-layer Ni(111) slab built by Xu et al. to investigate the graphene growth, including carbon dissolution, precipitation, and continuous growth.<sup>33</sup> Since there would be carbon dissolution into Ni-C solution and formation of graphitic C from Ni-C solution in our models, here we do not fix any layer of reactive solid

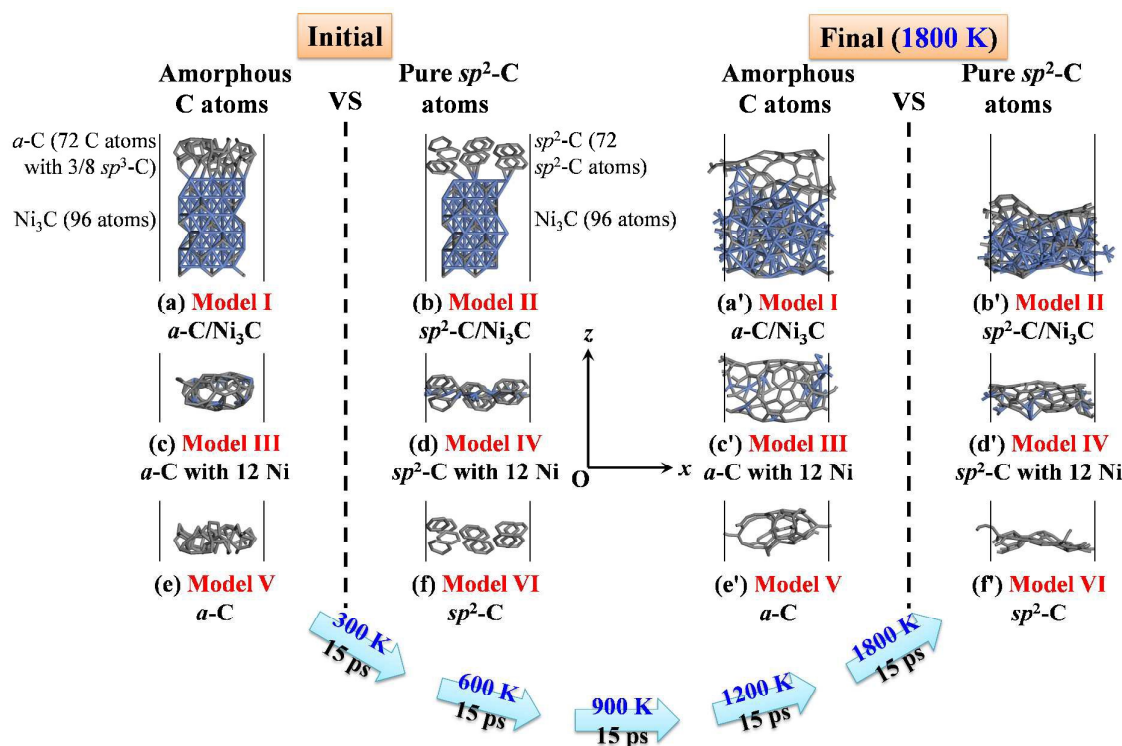


**Fig. 1** Initial (a–f) and final configurations of (a'–f') of Model I  $a$ -C/ $\text{Ni}_3\text{C}$ , Model II  $sp^2$ -C/ $\text{Ni}_3\text{C}$ , Model III  $a$ -C with 12 Ni, Model IV  $sp^2$ -C with 12 Ni, Model V  $a$ -C, and Model VI  $sp^2$ -C based on stepwise temperature increase from 300 K, 600 K, 900 K, 1200 K, to 1800 K every 15 ps in AIMD simulations. The Ni and C atoms are shown in blue and grey, respectively. The number of C atom or Ni atom in each model is also highlighted in insets. All the slab models are viewed along the surface  $y$  axis, and the vacuum layer along the  $z$  axis for each model is cut to highlight reactive solid layers.

layers. Model I and II are designed to understand the importance of the formation of  $\text{Ni}_3\text{C}$  phase in the RTP growth, considering the limited time scale for the AIMD simulations as it is impractical to simulate the whole series of dissolution of  $a$ -C into Ni, saturation of Ni with C, and diffusion of C in Ni, prior to the formation of nucleation site on the top surface. It is expected that the carbon cluster  $\text{C}_n$  species can be formed in the Ni-C solution before precipitation.<sup>36</sup> Thus, the precipitated  $\text{C}_n$  clusters can be  $sp^2/sp^3$ -mixed-C clusters or pure  $sp^2$ -C

clusters as shown in Fig. 1a and b. To further demonstrate the influence of  $\text{Ni}_3\text{C}$  formation on Ni easy evaporation and graphene formation in the RTP experiment, four new models (VIII to XI), including 72  $a$ -C and pure  $sp^2$ -C deposited on NiC [48 atoms, created based on Ni(111) surface replaced half number of atoms by C atoms] and pure Ni layers [72 atoms, created based on 3-layer Ni(111) surface], with decreased C content of supporting and catalyst layer, are built to make

comparison with Model I and II (see ESI Figs. S3-S5 and Table S1).

The Model III and IV (Fig. 1c and d) are designed to illustrate the catalysis effect of the Ni atoms and to further compare with Model I and II that contain  $\text{Ni}_3\text{C}$ . We notice that a recent study showed that the conversion of  $\alpha\text{-C}$  to graphene can occur without the Ni catalyst by annealing.<sup>48</sup> Model V and VI (Fig. 1e and f) are to draw comparison among all the models shown in Fig. 1. In addition for the Ni-catalyzed transformation of  $\alpha\text{-C}$  to graphene experiments, the formation of number of graphene layers can be tuned by changing the relative thicknesses of deposited  $\alpha\text{-C}$  and Ni thin films.<sup>43, 45, 47</sup> To further reproduce the dynamic growth process of the second graphene layer, we also build a model (Model VII graphene/ $\alpha\text{-C}/\text{Ni}_3\text{C}$ ) with one more fixed graphene layer (72 C atoms) deposited on the  $\alpha\text{-C}/\text{Ni}_3\text{C}$  layers to study the formation of the second graphene layer (see Fig. 8 as follows).

## 2.2 AIMD Simulations

To mimic the thermal heating process in the RTP experiment, eleven independent AIMD simulations are performed with the eleven model systems (Model I–VI in Fig. 1, Model VII in Fig. 8, and Model VIII–XI in ESI Fig. S3) in the *NVT* ensemble with the temperature (*T*) raised in every 15 ps step, from 300 K, to 600 K, 900 K, 1200 K, and the final 1800 K. Note that this rate of temperature increase is exceedingly faster than that in real experiments. As a result, the kinetics of growth becomes much more dominant than the thermodynamics.<sup>50</sup> Since the ultrafast growth rate in numerical simulations would induce kinetically trapped defects in the graphitic C structures,<sup>51</sup> the computational high-temperature annealing can be employed to accelerate the continuous graphene growth while at the same time reduce number of defects within graphene layer.<sup>51,52</sup> The temperature range of 1200 K to 1800 K covers the experiment temperature (1100°C) in RTP.<sup>47</sup> We also examined to increase growth temperature directly from 1200 K to 1800 K to accelerate the graphene growth, which did not notably alter the simulation results. Note also that the previous QM/MD simulations of the catalyst-free transformation of  $\alpha\text{-C}$  to graphene, the simulation temperature was increased from 600 K, 1200 K to 1800 K, while the energy change of the system still kept continuous.<sup>48</sup>

In addition, for Model I, the AIMD simulation is further carried out up to 2400 K and then to 3000 K, each with 15 ps, to examine post-annealing of the grown graphitic C structures. As a benchmark, four additional model systems are built (Fig. 3), including Ni bulk with 48 atoms, a graphene monolayer with 72 atoms, a  $\text{Ni}_3\text{C}$  slab, and a  $\text{Ni}(111)$  surface doped with C atoms (with 144 Ni atoms and 48 C atoms). For the four models, 15-ps, 25-ps, 50-ps, and 50-ps AIMD simulations are performed, respectively, all at 1200 K, to validate specific solid-liquid properties of nanoscale Ni-C solution by computing the mean square displacement (MSD)-time curves, and comparing with those of Ni bulk and perfect graphene.

All the AIMD simulations are performed within the framework of the Kohn–Sham formulation of DFT by using the GPW

method in the QUICKSTEP program of the CP2K software package. The PBE-D3 functional is employed with the cutoff radius of 20 Å for all dispersion calculations. A polarized double- $\xi$  quality Gaussian basis in conjunction with the norm-conserving Goedecker–Teter–Hutter (GTH) pseudopotential is used. The auxiliary plane-wave basis set is defined by an energy cutoff of 330 Ry, accompanied by a relative cutoff of 33 Ry for Gaussian basis set collocation. The self-consistent field (SCF) convergence is set to  $10^{-6}$  a.u. The time step in AIMD simulations is set as 1 fs. The temperature is controlled by a chain of Nosé–Hoover chain thermostat.

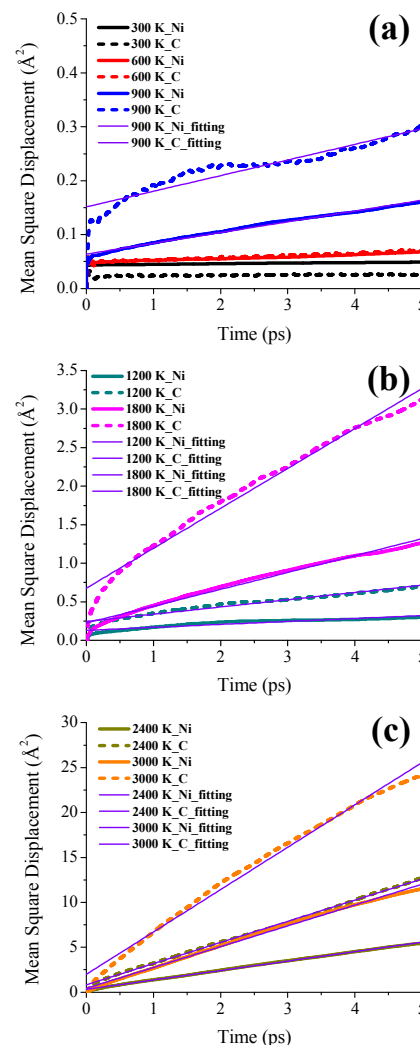


**Fig. 2** Variations of mean square displacement (MSD) with time of Ni (solid lines) and C (dashed lines) atoms in  $\text{Ni}_3\text{C}$  layer of Model I at (a) 300 K, 600 K, and 900 K, (b) 1200 K and 1800 K, and (c) 2400 K and 3000 K based on the AIMD simulations. The corresponding linear fitting of the MSD-time curves are in violet.

## 3. Results and discussion

After 75-ps stepwise-temperature-increase AIMD simulations, the final configurations of Model I–VI and Model VIII–XI are present in Fig. 1a'–f' and S3c'–f', respectively. As shown in Fig.



1a' and b', the graphitic layer and Ni<sub>3</sub>C layer tend to separate from each other. A few  $\alpha$ -C atoms can enter the Ni<sub>3</sub>C layer, while some surface Ni atoms stabilize the dangling C atoms in the graphitic layer. In addition, a two-layer graphitic structure is formed from  $\alpha$ -C with 3/8  $sp^3$ -C atoms on the Ni<sub>3</sub>C layer, while a relatively flat graphitic structure with a localized dome-like patch is formed from pure  $sp^2$ -C. Interestingly, the graphitic structure grown from the pure  $sp^2$ -C atoms is much flatter than that grown from the  $\alpha$ -C. Without the support of Ni<sub>3</sub>C layer, a carbon roll (Fig. 1c') and a carbon shell (Fig. 1e') are formed from  $\alpha$ -C, respectively, whereas a relatively flat graphitic structure is formed from pure  $sp^2$ -C (see Fig. 1d' and f'). The C structure in Fig. 1d' exhibits higher (concave) curvature compared to that in Fig. 1f'. Fig. 1c' and d' show that the catalysis effect of Ni atoms is important to the stabilization of the dangling C atoms by forming the  $\sigma$ -bonds besides dissolution of C atoms or supporting the newly-formed graphene. Moreover, after the formation of graphitic C structures, the Ni atoms tend to gather together, which can be attributed to the strongest C-C interaction among Ni-Ni, Ni-C, and C-C interactions in the Ni-C solution.<sup>36</sup> This result is also in line with the estimated formation energies of Ni-Ni, Ni-C, and C-C bonds given in ESI Fig. S1. For Model VIII  $\alpha$ -C/NiC and Model IX  $sp^2$ -C/NiC (ESI Fig. S3c' and d'), the final structures are quite similar to graphitic C structures shown in Fig. 1c' and d' due to the number of Ni atoms in the NiC layer is small, just twice of that of Model III and IV, resulting in decomposition of NiC layer in the end. Moreover, Ni atoms still prefer aggregation (see ESI Fig. S3c' and d'). For Model X  $\alpha$ -C/Ni and Model XI  $sp^2$ -C/Ni (ESI Fig. S3e' and f'), the graphitic C structures can be found to grow on Ni layers. The Ni layers still provides catalytic support to the grown C structures, the same as Ni<sub>3</sub>C layers in Model I and II. Remarkably, quite a few C atoms dissolve into the Ni layers in their final configurations.

**Table 1** Computed self-diffusion coefficients,  $D$  (unit:  $\text{cm}^2/\text{s}$ ), of Ni and C atoms in Ni<sub>3</sub>C layer of Model I at different temperatures (stepwise increase every 15 ps), and in Ni<sub>3</sub>C crystal and C-doped Ni(111) in Fig. 3c and d at 1200 K (50 ps) through linear fitting of MSD-time curves shown in Fig. 2 and Fig. 4c and d, respectively, on basis of AIMD simulations.

	900 K	1200 K	1800 K	2400 K	3000 K
<b>Ni<sub>3</sub>C layer of Model I</b>					
Ni	$3.3 \times 10^{-7}$	$6.4 \times 10^{-7}$	$3.7 \times 10^{-6}$	$1.8 \times 10^{-5}$	$3.9 \times 10^{-5}$
C	$4.8 \times 10^{-7}$	$1.6 \times 10^{-6}$	$8.6 \times 10^{-6}$	$3.9 \times 10^{-5}$	$7.9 \times 10^{-5}$
<b>Ni<sub>3</sub>C bulk crystal</b>					
Ni			$4.7 \times 10^{-7}$		
C			$1.5 \times 10^{-6}$		
<b>C-doped Ni(111)</b>					
Ni			$6.0 \times 10^{-7}$		
C			$1.6 \times 10^{-6}$		

### 3.1 Viscous-liquid-like Ni-C solution and faster diffusion of C atoms: easy evaporation of Ni in RTP growth of graphene

Based on computed MSDs of Ni and C atoms in the Ni<sub>3</sub>C layer of Model I at different temperatures, the role of Ni<sub>3</sub>C formation to the easy Ni evaporation can be analyzed. According to the Auger electron spectroscopy (AES) results in the recent RTP experiment,<sup>49</sup> the Ni<sub>3</sub>C intermediate forms in the temperature range of room temperature to 400°C. In addition, accompanied by the vanishing of Ni<sub>3</sub>C, the C atoms diffuse to the top surface at 800°C, and the bulk-to-surface diffusion of C atoms within Ni can be observed above 400°C.<sup>49</sup> Although the explicit  $\alpha$ -C diffusion to the top layer is not observed in our 75-ps AIMD simulations (separation between the graphitic layer and Ni<sub>3</sub>C layer in Fig. 1a'), the self-diffusion coefficient ( $D$ ) of Ni or C atoms in the Ni<sub>3</sub>C layer offers a guide to understand the specific phase behavior of nanoscale Ni-C solution. As shown in Fig. 2a, the MSD curves for Ni and C atoms in the Ni<sub>3</sub>C layer at 300 K and 600 K are nearly flat, indicating solid-like behavior of the Ni<sub>3</sub>C layer at both temperatures. At 600 K, the C and Ni atoms exhibit similar diffusion rates. From 900 K to 3000 K, the C atoms diffuse faster than the Ni atoms (see Fig. 2a–c). The self-diffusion coefficients of Ni and C atoms in the Ni<sub>3</sub>C layer (Table 1) are computed from the linear fitting of the MSD-time curves in Fig. 2. When the temperature is increased from 900 K to 1800 K, the diffusion coefficients are in the range of  $10^{-7}$ – $10^{-6}$   $\text{cm}^2/\text{s}$ , consistent with the previous experimental estimation of volume diffusion of C in Ni at 1100°C ( $D = D_0 \exp(-E/k_B T)$  where  $D_0 \approx 0.1$   $\text{cm}^2/\text{s}$ ,  $E \approx 1.5$  eV, and  $k_B$  is the Boltzmann constant.),<sup>53</sup> which indicates the Ni-C solution behaves like a *viscous liquid* in this temperature range (900–1800 K). The Ni-C solution behaves like a liquid when the temperature is higher than 2400 K (because the diffusion coefficients are higher than  $10^{-5}$   $\text{cm}^2/\text{s}$ ).

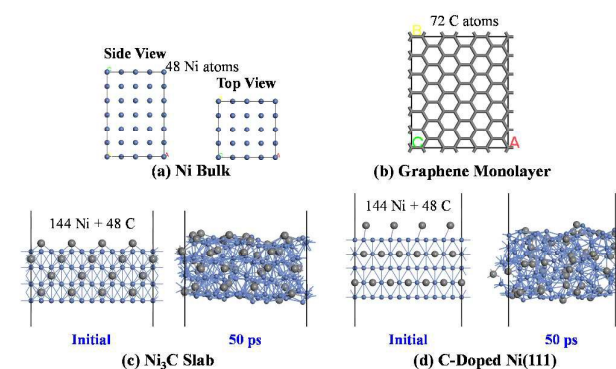


**Fig. 3** Four model systems: (a) Ni bulk, (b) graphene monolayer, (c) Ni<sub>3</sub>C slab (144 Ni and 48 C atoms), and (d) C-doped Ni(111) surface, used in the AIMD simulations at 1200 K. The 50-ps snapshots of Ni<sub>3</sub>C slab and C-doped Ni(111) are highlighted in the right panel in (c) and (d). The Ni and C atoms are shown in blue and grey, respectively.

To further confirm the phase behavior of Ni<sub>3</sub>C layer, four more model systems are built (see Fig. 3). Note that the surplus Ni with excess C atoms appears to evaporate at 1100°C in the experimental RTP growth of graphene.<sup>47</sup> The Ni bulk (Fig. 3a) and graphene monolayer (Fig. 3b) are taken as benchmark systems to confirm that both behave like a solid at 1200 K (which is slightly below the evaporation temperature 1100°C in

the RTP experiment<sup>47</sup>), as indicated by MSD-time curves (Fig. 4a and b) from our AIMD simulations. For the Ni<sub>3</sub>C slab model (carved from the bulk crystal, Fig. 3c) and the Ni(111) doped with C atoms (Fig. 3d), the diffusivity is investigated *via* 50-ps AIMD simulations at 1200 K. The system of Ni(111) doped with C atoms is generated from the Ni(111) thin film with some Ni atoms evenly replaced by C atoms so that the ratio of Ni to C is 3 to 1. Note that both model systems have more atoms than the Ni<sub>3</sub>C layer in Model I. As shown in Fig. 3c and d, the tendency for C atoms to diffuse onto the surface is still difficult to observe even after 50-ps AIMD simulations. The MSD-time curves are plotted every 10 ps after the initial 10-ps AIMD run (Fig. 4c and d). The computed diffusion coefficients shown in Table 1 (averaged over four MSD-time curves) are very close to the diffusion coefficients of the Ni<sub>3</sub>C layer in Model I at 1200 K and they suggest that the Ni-C solution at 1200 K behaves like a *viscous liquid*.

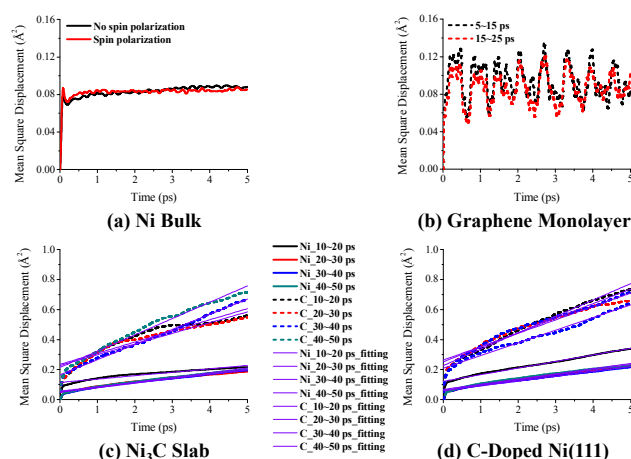


**Fig. 4** Variations of mean square displacement (MSD) with time of Ni atoms of (a) Ni bulk, C atoms of (b) graphene monolayer, and Ni and C atoms of (c) Ni<sub>3</sub>C slab and (d) C-doped Ni(111) surface at 1200 K based on the AIMD simulations. The corresponding linear fitting of the MSD-time curves are in violet. For Ni bulk, the non-spin-polarized and spin-polarized AIMD simulations are performed at 1200 K for comparison.

Furthermore, the phase behavior of Ni<sub>3</sub>C and graphene in Model I can be analyzed by the estimation of Lindemann Index ( $\delta$ ). A commonly used value that characterizes the solid/liquid phase transition is  $\delta = 0.1$ .<sup>40</sup> As shown in Fig. 5, the  $\alpha$ -C layer behaves like a solid in the whole temperature range of 300–3000 K, due to  $\delta < 0.09$ . When the temperature is higher than 2400 K,  $\delta$  of the Ni<sub>3</sub>C layer would be greater than 0.1 if the simulation time is long enough due to the transition to liquid phase.

At the nanoscale, the Ni-C solution and the pure Ni thin film exhibit different phase behavior from the bulk Ni and graphene C. As mentioned above, pure bulk Ni and graphene C behave like a solid at 1200 K. When C atoms are dissolved in Ni to form a Ni<sub>3</sub>C solution at 1200 K, the solution becomes viscous-liquid like. This viscous-liquid-like phase behavior can be also found in Ni-C solution with the ratio of Ni to C being 1 to 1, and pure Ni layer at 1200 K, as shown in ESI Fig. S4 and Table S1. For Model VIII  $\alpha$ -C/NiC and Model X  $\alpha$ -C/Ni (ESI Fig.

S4), the NiC and pure Ni layers behave like a solid at 300 K and 600 K, but viscous-liquid-like when the temperature is in the range of 900–1800 K, similar to the Ni<sub>3</sub>C layer in Model I. Notably, C atoms in the NiC layer (Model VIII) diffuse slightly faster than Ni atoms at all temperatures considered, except at 600 K. At 600 K, C atoms in the NiC layer diffuse much faster than Ni atoms. As shown ESI Table S1, diffusion coefficients of Ni or C atoms in the NiC layer (Model VIII) and in the Ni layer (Model X) have nearly the same order of magnitude as those in the Ni<sub>3</sub>C layer (Model I). Importantly, these diffusion coefficients of Ni or C atoms in the NiC and pure Ni layers are all slightly higher than those in the Ni<sub>3</sub>C layer, indicating that the viscous-liquid-like Ni<sub>3</sub>C at 900–1800 K may be more stable than either the NiC phase or the Ni thin film. That also supports the Auger electron spectroscopy (AES) measurement of the Ni<sub>3</sub>C phase from room temperature to 800°C, and the glancing-angle X-ray diffraction (GAXRD) measurement of RTP growth from 800°C to 1100°C.<sup>49</sup> Lindemann-index results for NiC, Ni, or  $\alpha$ -C layers in Model VIII  $\alpha$ -C/NiC and Model X  $\alpha$ -C/Ni (ESI Fig. S5) are similar to those of Model I  $\alpha$ -C/Ni<sub>3</sub>C (Fig. 5).

Different from previous studies of Ni-catalyzed transformation of  $\alpha$ -C to graphene,<sup>43–46</sup> the RTP growth entails a quite fast heating rate to induce direct Ni evaporation at an elevated temperature.<sup>47,49</sup> In reality, because of the rapid heating rate, a metastable Ni<sub>3</sub>C intermediate is found in the RTP experiment.<sup>47,49</sup> Based on our AIMD simulations, the viscous-liquid-like behavior of nanoscale Ni<sub>3</sub>C gives a possible explanation of the easy Ni evaporation at 1100°C in the RTP experiment, even though the Ni evaporation is not directly observed in the AIMD simulations due to limited time scale. In the realistic system,<sup>49</sup> the fast diffusion of C atoms (also being observed by our AIMD simulations) can be attributed to the formation of Ni<sub>3</sub>C layer as the temperature increases, and also contributes to the formation of Ni-C viscous liquid at an elevated temperature.

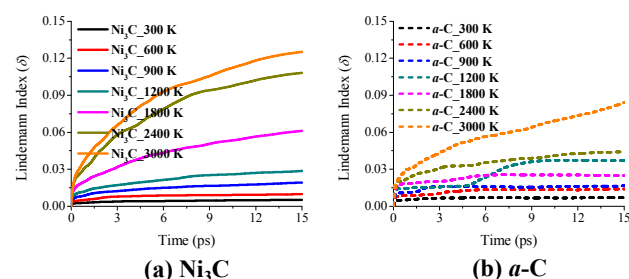


**Fig. 5** Lindemann index ( $\delta$ ) of (a) Ni<sub>3</sub>C layer and (b)  $\alpha$ -C layer in Model I, estimated from the 15-ps AIMD simulations with temperature increase from 300 K, 600 K, 900 K, 1200 K, 1800 K, 2400 K, to 3000 K.

### 3.2 Kinetically trapped graphitic structures in AIMD simulations

The simulations discussed above suggest that the graphene formation in the RTP growth follows the metal-induced crystallization and layer exchange mechanism proposed by Saenger *et al.*<sup>44</sup> The direct deposition of  $\alpha$ -C and  $sp^2$ -C layers

on the  $\text{Ni}_3\text{C}$  layer (Model I and II) can be used to show the evolvement of graphitic structures in the RTP experiment after precipitation as the temperature increases. The transformation of  $\alpha\text{-C}$  and  $\text{sp}^2\text{-C}$  into graphitic structures are summarized in Fig. 6. The  $\text{Ni}_3\text{C}$  layer or Ni atoms are omitted in Fig. 6 to illustrate only the temperature-dependent C structure evolvement of  $\alpha\text{-C}$  and  $\text{sp}^2\text{-C}$  in Model I–VI, where the temperature increase is from 300 K to 1800 K. In addition, C atoms in the five, six, and seven-membered rings within the  $\text{sp}^2\text{-C}$ -network are highlighted in green (others in grey). The integers in parenthesis below the C structures represent the numbers of five, six, and seven-membered rings within the  $\text{sp}^2$ -

C network. Since the rate of temperature increase in the AIMD simulations is exceedingly faster than that in real experiments, the condition of graphene growth is far from the equilibrium, and the kinetics of growth becomes much more dominant than the thermodynamics.<sup>50</sup> The ultrafast growth rate in numerical simulations would lead to kinetically trapped defects in the  $\text{sp}^2\text{-C}$  structures.<sup>51</sup> As shown in Fig. 6, the graphitic structures grown at 1800 K contain many non-hexagonal rings (polygonal defects). At this kinetic growth stage, the grown graphitic structures are C-source dependent as the structures evolved from  $\alpha\text{-C}$  with 3/8  $\text{sp}^3\text{-C}$  or from pure  $\text{sp}^2\text{-C}$  are markedly different.

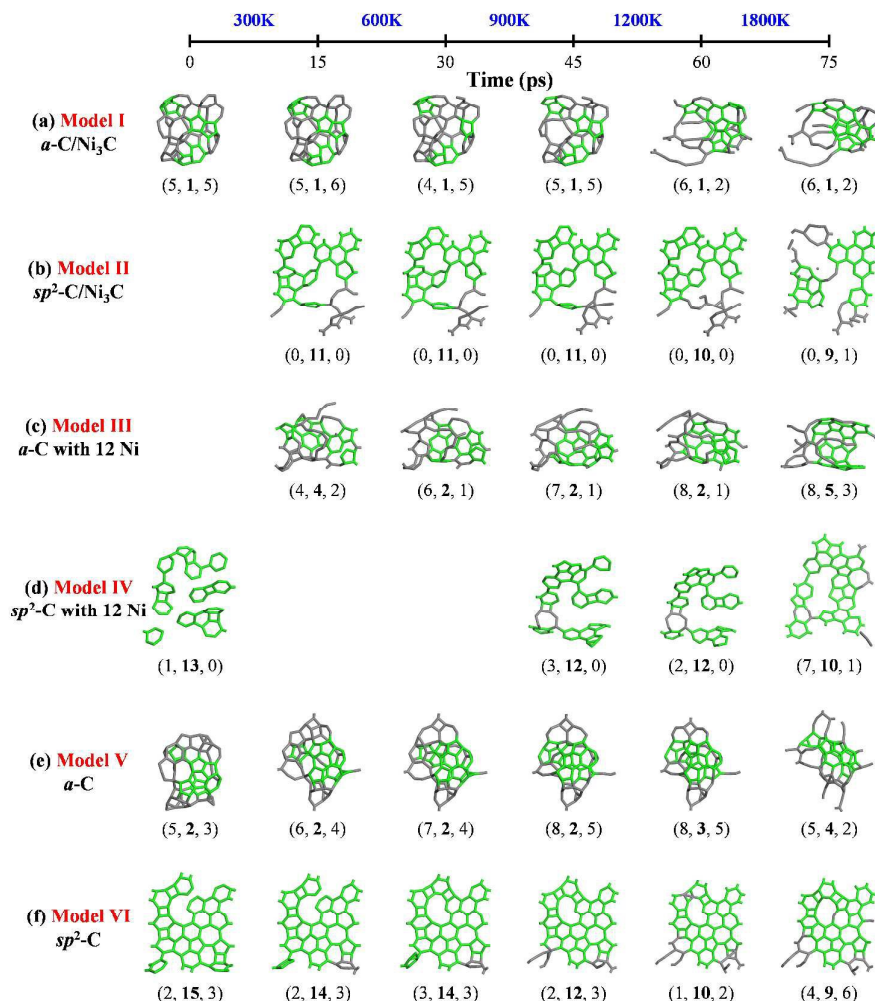


**Fig. 6** Temperature-dependent C structure evolvement of (a) Model I  $\alpha\text{-C}/\text{Ni}_3\text{C}$ , (b) Model II  $\text{sp}^2\text{-C}/\text{Ni}_3\text{C}$ , (c) Model III  $\alpha\text{-C}$  with 12 Ni, (d) Model IV  $\text{sp}^2\text{-C}$  with 12 Ni, (e) Model V  $\alpha\text{-C}$ , and (f) Model VI  $\text{sp}^2\text{-C}$  based on AIMD simulations with temperature increase every 15 ps from 300 K 600 K, 900 K, 1200 K, to 1800 K. C atoms of the  $\text{sp}^2\text{-C}$ -network-related five, six, and seven-membered rings are highlighted in green (the rest in grey). The numbers in bracket below the C structures indicates numbers of five, six, and seven-membered rings within the  $\text{sp}^2\text{-C}$  network. The  $\text{Ni}_3\text{C}$  layers are omitted in Model I and II and Ni atoms are omitted in Model III and IV to highlight the evolvement of C structures.

Although the  $\alpha\text{-C}$  layer in Model I, III, and V has a high fraction of  $\text{sp}^3\text{-C}$  atoms in the initial structures, those  $\text{sp}^3\text{-C}$  atoms are quickly converted to  $\text{sp}^2\text{-C}$  atoms after structure optimization and AIMD simulation even at room temperature (300 K). After 15-ps AIMD simulations at 300 K, the constituents of 5, 6, and 7-membered rings are nearly unchanged, compared with the

initial structures (Fig. 6a, c, and e), indicating that the energetically favorable 5, 6, and 7-membered rings stem from fused 5, 6, and 7-membered rings in the initial C clusters. These polygonal rings are kinetically trapped in the AIMD simulations. Upon temperature increase every 15 ps up to 1800 K, the constituents of the  $\text{sp}^2\text{-C}$  networks change a little,



but the  $sp^2$ -C networks gradually extend. In the  $\alpha$ -C layer of Model I, III, and V (Fig. 6a, c, and e), the number of 5-membered rings gradually increases, while the number of 6-membered rings changes a bit, and the number of 7-membered rings fluctuates as the temperature increases to 1200 K. From 1200 to 1800 K, the C structures exhibit notably more changes. In Model III (Fig. 6c), the numbers of 6- and 7-membered rings increase. In Model V (Fig. 6e), the numbers of 5- and 7-membered rings decrease while the number of 6-membered rings increases. Although the numbers of 5, 6, and 7-membered rings exhibit little change in Model I (Fig. 6a) at 1200 K and 1800 K, the  $sp^2$ -C networks contain C strings which would not arise in the C structures for  $T < 1200$  K, supporting the experimental observation of the reverse dissolution of graphitic C for  $T > 950^\circ\text{C}$ .<sup>44</sup> Compared to the grown C structures in Model III and V (Fig. 6c and e) which contain less C strings at 1200 K and 1800 K, one can conclude that the  $\text{Ni}_3\text{C}$  layer can stabilize newly formed C strings while re-dissolve the graphitic structures at high temperatures.

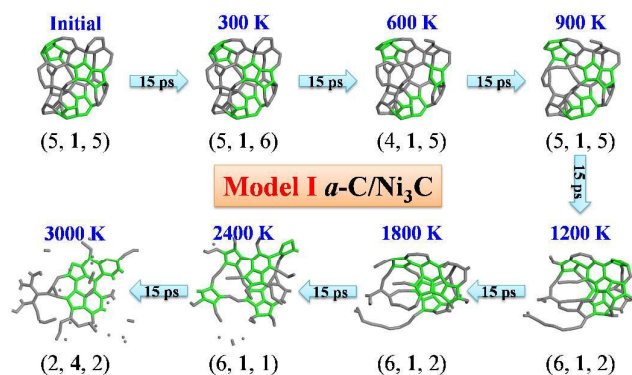


**Fig. 7** Temperature-dependent C structure evolution of Model I  $\alpha$ -C/ $\text{Ni}_3\text{C}$  based on AIMD simulations with temperature increase every 15 ps from 300 K, 600 K, 900 K, 1200 K, 1800 K, 2400 K, to 3000 K. C atoms of the  $sp^2$ -C-network-related five, six, and seven-membered rings are highlighted in green (the rest in grey). The numbers in bracket below the C structures indicates numbers of five, six, and seven-membered rings within the  $sp^2$ -C network. The  $\text{Ni}_3\text{C}$  layer is omitted here to highlight the evolution of C structures.

In the pure  $sp^2$ -C layer of Model II, IV, and VI (Fig. 6b, d, and f), the grown C structures are all restively flat at different temperatures, unlike the structures of carbon rolls or shell out of the  $\alpha$ -C layer in the case of Model I, III, and V. The fused 6-membered rings are also originated from the initial pure  $sp^2$ -C. From 1200 K to 1800 K, the C structures of the  $sp^2$ -C layer also undergo slightly more changes like those in the case of the  $\alpha$ -C layer. The numbers of fused 6-membered rings decrease while the numbers of 5 and 7-membered rings increase. These results are consistent with the experimental observation that the grown graphitic C would reversibly dissolve for  $T > 950^\circ\text{C}$ .<sup>44</sup> As shown in Fig. 7, we have performed additional AIMD simulations on the structure of Model I with temperature raised from 1800 K to 2400 K and then to 3000 K, each for 15 ps to visualize the possible defect healing in real experiment. At 2400 K, isolated C atoms start to appear and the  $sp^2$ -C network exhibits some changes. At 3000 K isolated C atoms

spring up, indicating further reverse dissolution of graphitic structures in Ni. However, the  $sp^2$ -C core exhibits increasing number of 6-membered rings. Apparently, the ultrahigh temperature can remove the defects in the  $sp^2$ -C network, consistent with the results from a previous tight-binding MC simulation of isolated graphene.<sup>51</sup> However, the high temperature can also induce the reverse dissolution of graphitic C when the catalyst metal coexists.

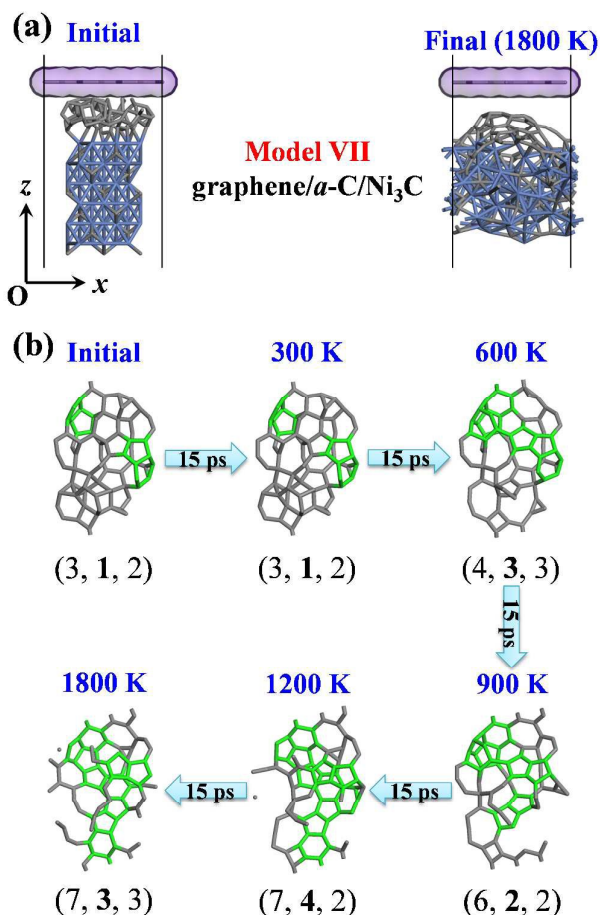


**Fig. 8** (a) Initial and final configurations, viewed along the  $y$  axis, and (b) temperature-dependent C structure evolution of Model VII graphene/ $\alpha$ -C/ $\text{Ni}_3\text{C}$  based on AIMD simulations with temperature increase every 15 ps from 300 K, 600 K, 900 K, 1200 K, to 1800 K. For (a), the Ni and C atoms are shown in blue and grey, respectively. The perfect first graphene layers are also highlighted with purple vdW surface. The vacuum layer along the  $z$  axis is cut to highlight reactive solid layers (the whole super cell is depicted in ESI Fig. S2b). For (b), the  $\text{Ni}_3\text{C}$  layer is omitted to highlight the evolution of C structures. C atoms of the  $sp^2$ -C-network-related five, six, and seven-membered rings are highlighted in green (the rest in grey). The numbers in bracket below the C structures indicates numbers of five, six, and seven-membered rings within the  $sp^2$ -C network.

### 3.3 Formation of the orderly carbon core in the second graphene layer

In the metal-catalyzed transformation of  $\alpha$ -C to graphene experiments, the formation of number of graphene layers can be tuned by altering thicknesses of deposited  $\alpha$ -C and Ni thin films.<sup>43, 45, 47</sup> In Ni-catalyzed CVD growth of graphene, when the

Ni(111) surface is covered with a graphene monolayer that is in registry with the underlying Ni, the formation of additional graphene layer is prevented at low exposure pressure, leading the self-limiting graphene growth behavior.<sup>54</sup> When the quantity of  $\alpha$ -C is abundant, the mechanism of Ni-catalyzed transformation of  $\alpha$ -C to graphene differs from the self-limiting one. The graphene growth in the RTP experiment appears to follow the metal-induced crystallization and layer exchange mechanism. The grown graphene on the surface of Ni-C solution can further promote continued dissolution of the  $\alpha$ -C layer.<sup>44</sup> Even after the surface of Ni-C solution is entirely covered by a graphene layer, the replenished C clusters by continued dissolution of abundant  $\alpha$ -C can give rise to new nucleation sites to further grow the second layer of graphene. To support this view, we build a new model (Model VII graphene/ $\alpha$ -C/ $\text{Ni}_3\text{C}$ ) with one more graphene layer deposited on the  $\alpha$ -C/ $\text{Ni}_3\text{C}$  layers to study the formation of the second graphene layer (see Fig. 8). Here, the first perfect graphene layer is fixed in the AIMD simulations. As shown in Fig. 8a, a dome-like graphitic C structure forms between the graphene layer and  $\text{Ni}_3\text{C}$  layer. This newly formed  $sp^2$ -C network in Fig. 8 appears to be more orderly than that without the first graphene layer coating, as compared to the grown C structure from Model I (Fig. 1a' and 6a). As shown in Fig. 8b, the numbers of 5, 6, and 7-membered rings in the second  $sp^2$ -C network of Model VII are more than those in the C structure of Model I (Fig. 6a). It seems the first graphene layer could accelerate the formation of orderly C core in the second graphitic layer.

#### 4. Conclusions

We have performed comprehensive AIMD simulations to investigate atomic-scale mechanism of Ni evaporation and graphene formation in the RTP growth of graphene. Our simulations suggest that the easy evaporation of Ni at 1100°C in the RTP experiment is likely due to the formation of viscous-liquid-like Ni-C solution (even at 900 K), a phase behavior specific to the nano-scale Ni-C system. The graphitization in the RTP growth follows the Ni-induced crystallization and layer exchange mechanism. C atoms in Ni have low concentration and relatively high diffusion rate. When the temperature is higher than 600 K, C atoms diffuse faster than Ni atoms in the Ni-C solution. The graphitic C formation can start at low temperature. Even at 300 K, the  $sp^3$ -C atoms no longer exist. The main  $sp^2$ -C-network-related structures, i.e., 5, 6, and 7-membered rings, as nucleation sites, stem from fused 5, 6, and 7-membered rings of initial C clusters precipitated from the Ni-C solution. In the kinetic growth stage of the RTP experiment, the grown C structures depend on the C sources (either  $sp^3$ -C or  $sp^2$ -C). Since the rate of temperature increase in the AIMD simulations is exceedingly faster than in the real experiments, the grown graphitic structures in the simulations contain many kinetically "trapped" defects. The grown graphitic structures from  $\alpha$ -C with  $sp^3$ -C atoms tend to form carbon rolls or carbon shells, while the grown graphitic structures from pure  $sp^2$ -C tend to form flat haeckelites. With the presence of the first

graphene layer, new nucleation sites for growing the second graphene layer can quickly form from the Ni-C solution. In the RTP experiment, the Ni catalyst can stabilize the dangling C atoms, dissolve C atoms, and support the newly-grown flat graphene. When the temperature is as high as 1200 K, the grown graphitic structures can reversely dissolve. In the AIMD simulations, the kinetically trapped defects in the graphitic structure can be healed at ultrahigh temperature. However, with metal catalyst, the ultrahigh temperature can reversely dissolve the grown graphitic structure.

#### Acknowledgements

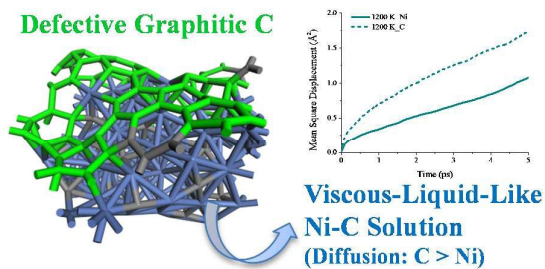
This work was supported by a grant from Nebraska Center for Energy Sciences Research in the University of Nebraska-Lincoln and by the University of Nebraska Holland Computing Center.

#### Notes and references

- 1 A. K. Geim and K. S. Novoselov, *Nature Mater.*, 2007, **6**, 183-191.
- 2 A. K. Geim, *Science*, 2009, **324**, 1530-1534.
- 3 K. S. Novoselov, V. I. Fal'ko, L. Colombo, P. R. Gellert, M. G. Schwab and K. Kim, *Nature*, 2012, **490**, 192-200.
- 4 K. S. Novoselov, D. Jiang, F. Schedin, T. J. Booth, V. V. Khotkevich, S. V. Morozov and A. K. Geim, *Proc. Natl. Acad. Sci.*, 2005, **102**, 10451-10453.
- 5 Y. Hernandez, V. Nicolosi, M. Lotya, F. M. Blighe, Z. Sun, S. De, I. T. McGovern, B. Holland, M. Byrne, Y. K. Gun'ko, J. J. Boland, P. Niraj, G. Duesberg, S. Krishnamurthy, R. Goodhue, J. Hutchison, V. Scardaci, A. C. Ferrari and J. N. Coleman, *Nature Nanotech.*, 2008, **3**, 563-568.
- 6 S. Park and R. S. Ruoff, *Nature Nanotech.*, 2009, **4**, 217-224.
- 7 D. R. Dreyer, S. Park, C. W. Bielawski and R. S. Ruoff, *Chem. Soc. Rev.*, 2010, **39**, 228-240.
- 8 C. Berger, Z. Song, X. Li, X. Wu, N. Brown, C. Naud, D. Mayou, T. Li, J. Hass, A. N. Marchenkov, E. H. Conrad, P. N. First and W. A. de Heer, *Science*, 2006, **312**, 1191-1196.
- 9 K. V. Emtsev, A. Bostwick, K. Horn, J. Jobst, G. L. Kellogg, L. Ley, J. L. McChesney, T. Ohta, S. A. Reshanov, J. Rohrl, E. Rotenberg, A. K. Schmid, D. Waldmann, H. B. Weber and T. Seyller, *Nature Mater.*, 2009, **8**, 203-207.
- 10 K. S. Kim, Y. Zhao, H. Jang, S. Y. Lee, J. M. Kim, K. S. Kim, J.-H. Ahn, P. Kim, J.-Y. Choi and B. H. Hong, *Nature*, 2009, **457**, 706-710.
- 11 A. Reina, X. Jia, J. Ho, D. Nezich, H. Son, V. Bulovic, M. S. Dresselhaus and J. Kong, *Nano Lett.*, 2009, **9**, 30-35.
- 12 X. Li, W. Cai, J. An, S. Kim, J. Nah, D. Yang, R. Piner, A. Velamakanni, I. Jung, E. Tutuc, S. K. Banerjee, L. Colombo and R. S. Ruoff, *Science*, 2009, **324**, 1312-1314.
- 13 R. S. Edwards and K. S. Coleman, *Acc. Chem. Res.*, 2013, **46**, 23-30.
- 14 K. Yan, L. Fu, H. Peng and Z. Liu, *Acc. Chem. Res.*, 2013, **46**, 2263-2274.
- 15 Y. Zhang, L. Zhang and C. Zhou, *Acc. Chem. Res.*, 2013, **46**, 2329-2339.
- 16 X. Li, W. Cai, L. Colombo and R. S. Ruoff, *Nano Lett.*, 2009, **9**, 4268-4272.
- 17 W. Zhang, P. Wu, Z. Li and J. Yang, *J. Phys. Chem. C*, 2011, **115**, 17782-17787.
- 18 G. Gajewski and C.-W. Pao, *J. Chem. Phys.*, 2011, **135**, 064707.
- 19 K. Li, C. He, M. Jiao, Y. Wang and Z. Wu, *Carbon*, 2014, **74**, 255-265.

- 20 W. Chen, H. Chen, H. Lan, P. Cui, T. P. Schulze, W. Zhu and Z. Zhang, *Phys. Rev. Lett.*, 2012, **109**, 265507.
- 21 Y. Huang, J. Du, T. Zhou, C. Ling, S. Wang and B. Geng, *ACS Catal.*, 2014, **4**, 892-902.
- 22 J. Gao, J. Yip, J. Zhao, B. I. Yakobson and F. Ding, *J. Am. Chem. Soc.*, 2011, **133**, 5009-5015.
- 23 Q. Yuan, J. Gao, H. Shu, J. Zhao, X. Chen and F. Ding, *J. Am. Chem. Soc.*, 2012, **134**, 2970-2975.
- 24 J. Gao, J. Zhao and F. Ding, *J. Am. Chem. Soc.*, 2012, **134**, 6204-6209.
- 25 H. Shu, X. Chen, X. Tao and F. Ding, *ACS Nano*, 2012, **6**, 3243-3250.
- 26 L. Wang, X. Zhang, H. L. W. Chan, F. Yan and F. Ding, *J. Am. Chem. Soc.*, 2013, **135**, 4476-4482.
- 27 X. Zhang, L. Wang, J. Xin, B. I. Yakobson and F. Ding, *J. Am. Chem. Soc.*, 2014, **136**, 3040-3047.
- 28 L. Meng, Q. Sun, J. Wang and F. Ding, *J. Phys. Chem. C*, 2012, **116**, 6097-6102.
- 29 L. Meng, J. Jiang, J. Wang and F. Ding, *J. Phys. Chem. C*, 2014, **118**, 720-724.
- 30 Y. Lu and X. Yang, *Carbon*, 2015, **81**, 564-573.
- 31 P. Wu, H. Jiang, W. Zhang, Z. Li, Z. Hou and J. Yang, *J. Am. Chem. Soc.*, 2012, **134**, 6045-6051.
- 32 Z. Liang, Z. Xu, T. Yan and F. Ding, *Nanoscale*, 2014, **6**, 2082-2086.
- 33 Z. Xu, T. Yan, G. Liu, G. Qiao and F. Ding, *Nanoscale*, 2016, **8**, 921-929.
- 34 E. C. Neyts, A. C. T. v. Duin and A. Bogaerts, *Nanoscale*, 2013, **5**, 7250-7255.
- 35 Y. Wang, A. J. Page, Y. Nishimoto, H.-J. Qian, K. Morokuma and S. Irle, *J. Am. Chem. Soc.*, 2011, **133**, 18837-18842.
- 36 H.-B. Li, A. J. Page, Y. Wang, S. Irle and K. Morokuma, *Chem. Commun.*, 2012, **48**, 7937-7939.
- 37 A. J. Page, Y. Wang, H.-B. Li, S. Irle and K. Morokuma, *J. Phys. Chem. C*, 2013, **117**, 14858-14864.
- 38 M. Jiao, H. Qian, A. Page, K. Li, Y. Wang, Z. Wu, S. Irle and K. Morokuma, *J. Phys. Chem. C*, 2014, **118**, 11078-11084.
- 39 Y. Wang, A. J. Page, H.-B. Li, H.-J. Qian, M.-g. Jiao, Z.-J. Wu, K. Morokuma and S. Irle, *Nanoscale*, 2014, **6**, 140-144.
- 40 H.-B. Li, A. J. Page, C. Hettich, B. a. Aradi, C. Köhler, T. Frauenheim, S. Irle and K. Morokuma, *Chem. Sci.*, 2014, **5**, 3493-3500.
- 41 Özçelik, S. Cahangirov and S. Ciraci, *Phys. Rev. B*, 2012, **85**, 235456.
- 42 Y. Shibuta, R. Arifin, K. Shimamura, T. O. F. Shimojo and S. Yamaguchi, *Chem. Phys. Lett.*, 2013, **565**, 92-97.
- 43 M. Zheng, K. Takei, B. Hsia, H. Fang, X. Zhang, N. Ferralis, H. Ko, Y.-L. Chueh, Y. Zhang, R. Maboudian and A. Javey, *Appl. Phys. Lett.*, 2010, **96**, 063110.
- 44 K. L. Saenger, J. C. Tsang, A. A. Bol, J. O. Chu, A. Grill and C. Lavoie, *Appl. Phys. Lett.*, 2010, **96**, 153105.
- 45 C. M. Orofeo, H. Ago, B. Hu and M. Tsuji, *Nano Res.*, 2011, **4**, 531-540.
- 46 J. A. Rodríguez-Manzo, C. Pham-Huu and F. Banhart, *ACS Nano*, 2011, **5**, 1529-1534.
- 47 W. Xiong, Y. S. Zhou, L. J. Jiang, A. Sarkar, M. Mahjouri-Samani, Z. Q. Xie, Y. Gao, N. J. Ianno, L. Jiang and Y. F. Lu, *Adv. Mater.*, 2013, **25**, 630-634.
- 48 A. Barreiro, F. Börrnert, S. M. Avdoshenko, B. Rellinghaus, G. Cuniberti, M. H. Rummeli and L. M. K. Vandersypen, *Sci. Rep.*, 2013, **3**, 1115.
- 49 W. Xiong, Y. S. Zhou, W. J. Hou, T. Guillemet, J.-F. Silvain, Y. Gao, M. Lahaye, E. Lebraud, S. Xu, X. W. Wang, D. A. Cullen, K. L. More, L. Jiang and Y. F. Lu, *RSC Adv.*, 2015, **5**, 99037-99043.
- 50 X. Zhang, H. Li and F. Ding, *Adv. Mater.*, 2014, **26**, 5488-5495.
- 51 S. Karoui, H. Amara, C. Bichara and F. Ducastelle, *ACS Nano*, 2010, **4**, 6114-6120.
- 52 M. Jiao, W. Song, H.-J. Qian, Y. Wang, Z. Wu, S. Irle and K. Morokuma, *Nanoscale*, 2016, **8**, 3067-3074.
- 53 E.V. Rut'kov and N.R. Gall, Equilibrium Nucleation, Growth, and Thermal Stability of Graphene on Solids, in *Physics and Applications of Graphene – Experiments*, ed. S. Mikhailov, ISBN: 978-953-307-217-3, InTech, 2011, pp 209–292.
- 54 R. S. Weatherup, H. Amara, R. Blume, B. Dlubak, B. C. Bayer, M. Diarra, M. Bahri, A. Cabrero-Vilatela, S. Caneva, P. R. Kidambi, M.-B. Martin, C. Deranlot, P. Seneor, R. Schloegl, F. Ducastelle, C. Bichara and S. Hofmann, *J. Am. Chem. Soc.*, 2014, **136**, 13698-13708.

## Graphical Abstract



Fast formation of defective graphitic C structure and easy evaporation of surplus Ni atoms with excess C atoms are likely attributed to the formation of *viscous-liquid-like* Ni-C solution and faster diffusion of C atoms in Ni at 1200 K.